Materials Advances

ROYAL SOCIETY OF CHEMISTRY

PAPER

View Article Online
View Journal | View Issue

Cite this: *Mater. Adv.*, 2024, 5, 3915

BODIPY-cucurbituril complexes: supramolecular approach toward improvement of photodynamic activity†

Jiri Demuth, ‡[a] Rahul Kaushik, §‡[a] Magdalena Kozlikova, ‡[a] Carola Rando, [b] Miloslav Machacek, [a] Veronika Novakova, [a] Vladimír Šindelář *[b] and Petr Zimcik *[a]

Received 22nd December 2023,
Accepted 9th March 2024

DOI: 10.1039/d3ma01164j

rsc.li/materials-advances

The host–guest interaction of cucurbit[7]uril with lipophilic BODIPYs decreases their aggregation in water and improves the photophysical properties. Phototoxicity of the complex with one CB[7] moiety increased up to seven times compared to that of the free photosensitizer. This supramolecular interaction is an efficient approach to increasing the photodynamic activity of BODIPY photosensitizers.

Solubilization of lipophilic drugs by the formation of host–guest assemblies with hydrophilic hosts is among the applications utilized for improving physicochemical properties, activity, controlled release under specific conditions, or targeting of the drugs including those used in photodynamic therapy (PDT).[1–6] PDT is a method of treatment of various cancerous conditions based on the production of cytotoxic species (singlet oxygen) upon the activation of a photosensitizer (PS) by light of suitable wavelength. PSs recruit from various structural types (porphyrins, chlorins, phthalocyanines, and boron-dipyrromethens (BODIPYs)).[7] In all cases, the PSs suffer from aggregation of large hydrophobic macrocyclic cores that turn them into photophysically inactive forms with low fluorescence and singlet oxygen production. Besides modification of the structures with hydrophilic substituents, the above-mentioned supramolecular approaches have attempted to improve the water-solubility and photodynamic activity of PS. Highly hydrophilic cyclodextrins and cucurbit[*n*]urils (CB[*n*]) were mostly utilized for the solubilization of various PS.[8] For example, CB[7], known to form stable inclusion complexes with organic cations, was used to increase water solubility and reduce aggregation of phthalocyanine,[9] porphyrin,[10] or methylene blue[11] PSs with various consequences (positive or negative) for the final photodynamic activity. Also, an opposite approach in delivering AIEgens (aggregation-induced emission fluorophores) attached to CB[7] was recently reported.[12]

BODIPY dyes are among the widely investigated compounds in biomedicine, including PDT.[13] Their interactions with CB[*n*]s are, however, rather limited[14–18] and any improvement in photodynamic activity by host–guest interactions has not yet been reported with the exception of improved self-degradation.[19] In this work, we focused our attention on PSs derived from BODIPYs with substituents (in the *meso* position or on styryls) that allow host–guest interactions with one or two CB[7] molecules. These self-assembled supramolecular PSs were expected to have improved photophysical parameters and consequently also photodynamic activity.

In our project, we have taken into account the following rational considerations (Fig. 1A): (a) dipyrromethene core has been substituted at positions 2 and 6 by iodine atoms that are known to increase intersystem crossing by heavy-atom effect[20] and thus also induced singlet oxygen production. (b) *meso*-Aryl substituted tetramethyl BODIPYs typically absorb slightly above 500 nm and are not very suitable for PDT where the light of wavelengths below 630 nm is absorbed by endogenous chromophores and its penetration through human tissues is strongly limited. For this reason, positions 3 and 5 were modified by styryls that extend the conjugated system with an important red shift of the absorption band. (c) 1-Aminoadamantane and its analogues substituted on nitrogen atoms are known to form strong host–guest complexes with CB[7] having K_a values in the range of 10^{12}–10^{15} M^{-1}.[9,21,22] Therefore, adamantyl (Ad) substituents have been placed on either *meso* position (**1–3**, one Ad) or on both styryl substituents (**4** and **5**, two Ads). This allowed us to evaluate the effect of one or two bulky and hydrophilic CB[7]

[a] *Charles University, Faculty of Pharmacy in Hradec Kralove, Ak. Heyrovskeho 1203, Hradec Kralove, 50005, Czech Republic. E-mail: zimcik@faf.cuni.cz*
[b] *Department of Chemistry and RECETOX, Faculty of Science, Masaryk University, Kamenice 5, 625 00 Brno, Czech Republic. E-mail: sindelar@chemi.muni.cz*

† Electronic supplementary information (ESI) available: Experimental details, NMR spectra,HPLC traces, additional figures from biological evaluation. See DOI: https://doi.org/10.1039/d3ma01164j.

‡ Jiri Demuth, Rahul Kaushik and Magdalena Kozlikova have contributed equally to this work.

§ Current address: Chemical Oceanography Division, CSIR, National Institute of Oceanography, Dona Paula 403004, Goa, India.

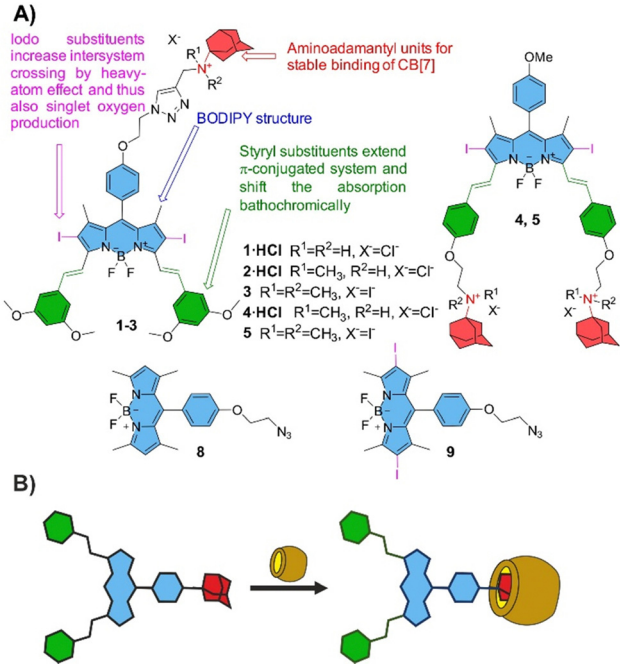

Fig. 1 (A) Structures of target BODIPYs **1–5** investigated in this work with the rationale behind the design. (B) Schematic principle of the interaction of BODIPY with CB[7].

molecules on the final BODIPY properties after the inclusion of Ad inside the macrocycle (Fig. 1B).

To obtain the desired PSs, multi-step synthesis started by acid-catalyzed condensation of 2,4-dimethylpyrrole with corresponding aromatic aldehydes, followed by oxidation, boron complexation and subsequent iodination using *N*-iodosuccinimide. Further, for the introduction of styryl moieties, Knoevenagel condensation was carried out in toluene in the presence of piperidine, and catalytic amounts of $Mg(ClO_4)_2$ and *p*-toluenesulfonic acid using a Dean–Stark condenser. The aminoadamantyl moieties in compounds **1** and **2** were introduced by Cu-catalyzed azide–alkyne cycloaddition reaction between azido-BODIPY and propargylaminoadamantyls. Quaternization of tertiary amines in **2** and **4** by methyl iodide provided corresponding **3** and **5** almost quantitatively. Finally, BODIPYs **1**, **2** and **4** were also converted into corresponding hydrochlorides (dihydrochloride for **4**) (further indicated as **1·HCl**, **2·HCl** and **4·HCl**) to improve at least slightly their solubility in water. For full details on the synthesis see ESI† and Schemes S1 and S2.

Absorption spectra of target BODIPYs were first measured in DMF (Fig. 2A) and were characterized by a sharp Q-band indicating that the compounds were essentially non-aggregated in this solvent. Additionally, the perfect overlap of the absorption and excitation spectra further confirmed the presence of a monomeric form (Fig. 2B and Fig. S1, ESI†). The position of the main absorption maximum (Table 1, Fig. 2A) shifted from λ_{max} = 500 nm for tetramethyl BODIPY **8** (noniodinated ancestor of **9**) for 33 nm upon iodination with λ_{max} = 533 nm for **9**. Compounds **8** and **9** were available as synthetic intermediates during the synthesis of **1–3** (see Scheme S1, ESI†). Extension of

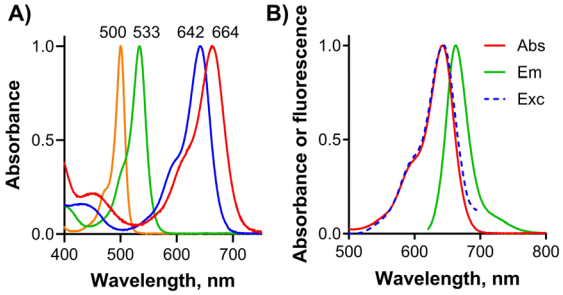

Fig. 2 (A) Normalized absorption spectra of **8** (orange), **9** (green), **2** (blue) and **4** (red) in DMF (c = 1 μM), indicating the spectral shift upon iodination and styryl attachment. (B) Normalized absorption (red), emission (green) and excitation (blue, dashed) spectra of **3** in DMF.

Table 1 Photophysical data of studied BODIPYs in DMF and log *P* values[a]

Cpd.	λ_{max} (log ε), nm	λ_{em}	τ_F, ns	Φ_F[b]	Φ_Δ[c]	log *P*	log *P* + CB[7][d]
1	642 (4.87)	662	1.43	0.21	0.51	—	—
1·HCl	643 (4.94)	662	1.48	0.21	0.45	2.41	1.98
2	642 (4.99)	662	1.41	0.21	0.50	—	—
2·HCl	641 (4.76)	661	1.44	0.23	0.50	2.38	2.35
3	643 (5.01)	663	1.42	0.21	0.53	2.06	1.28
4	664 (4.87)	688	0.43 (84%), 1.12 (16%)	0.058[e]	0.12	—	—
4·HCl	662 (4.90)	681	0.47 (74%), 1.69 (26%)	0.056	0.11	1.88	1.88
5	656 (4.89)	679	1.61	0.18	0.42	2.13	0.23
8	500 (4.85)	507[f]	2.85[f]	0.61[f]	0.034[f]	—	—
9	533 (4.90)	548[f]	0.15[f]	0.020[f]	0.65[f]	—	—

[a] Absorption maximum, λ_{max}; extinction coefficient, ε; emission maximum, λ_{em}; fluorescence lifetime, τ_F; fluorescence quantum yield, Φ_F; singlet oxygen quantum yield, Φ_Δ; partition coefficient between *n*-octanol and PBS, *P*. [b] Reference: ZnPc in THF (Φ_F = 0.32) for **1–5** and rhodamine G6 in EtOH (Φ_F = 0.94) for **8** and **9**. [c] Reference: ZnPc in DMF (Φ_Δ = 0.56) for **1–5** and bengal rose in MeOH (Φ_Δ = 0.76). [d] In the presence of 2 equiv. of CB[7] per one Ad moiety. [e] Φ_F = 0.25 and τ_F = 1.66 ns were determined in DMF in the presence of 64 μM HCl. [f] In MeOH.

the π-conjugated system with styryls further shifted to the absorption toward the longer wavelengths. Those BODIPYs substituted with methoxy groups in *meta* positions on styryls absorbed around 642 nm (**1–3**) while conjugation of the alkoxy group in the *para* position shifted the absorption further bathochromically to around 660 nm (**4**, **5**).

BODIPYs are well-known fluorophores with typically high fluorescence quantum yields (Φ_F) but a rather low singlet oxygen quantum yields (Φ_Δ) as exemplified in this work on the synthetic intermediate **8** with Φ_F = 0.61 and Φ_Δ = 0.034 (Table 1). Iodination (due to the heavy-atom effect) in **9** switched the deactivation pathways of the excited state toward singlet oxygen formation (Φ_F = 0.020 and Φ_Δ = 0.61). Styryl attachment reduced slightly the effect of iodination (it must affect larger molecules) and BODIPYs **1–3** and **5** were characterized by $\Phi_F \sim 0.21$ and still high $\Phi_\Delta \sim 0.50$ that are ideal for PDT and at the same time also for visualization of the BODIPYs inside the cells (Table 1). All of these compounds were further characterized by fluorescence lifetimes $\tau_F \sim 1.4$–1.5 ns with

monoexponential decays. The only exception was **4** containing two tertiary amino groups with substantially lower Φ_F and Φ_Δ and biexponential decay with a predominant fast component (Table 1). An explanation of this behavior may be found in the photoinduced electron transfer (PET) from amino groups (donor). This has been further confirmed by titration with HCl (Fig. S4, ESI†) resulting in negligible changes in absorption spectra, restoration of fluorescence (Φ_F = 0.25) and lifetime τ_F = 1.66 ns with only monoexponential decay as a consequence of a block of lone pair needed for PET. Interestingly, the presence of two amine donors in the molecule seems to be essential for efficient PET quenching in DMF as no such observations were detected for compounds **1** and **2** with one amine in the *meso* position or for compounds with only one aliphatic amine on styryl, as reported in literature.[2,3]

The investigated compounds (even in the form of hydrochlorides) were not directly soluble in water or PBS. When the DMF stock solution was added to PBS, large aggregates were formed with very low absorption and no fluorescence emission. The addition of CB[7] into pure PBS slowly increased fluorescence emission but the changes were very slow and it took a couple of hours to see some spectral changes. For this reason, the effect of CB[7] interaction with BODIPYs on their photophysics was investigated in PBS containing 20% of MeCN where the changes were better observable. Still, the fluorescence experiments were complicated by unexpectedly slow host–guest equilibration taking about 2–3 hours (Fig. S3, ESI†). We attributed this behavior to the formation of BODIPYs aggregates in water from which the monomers were slowly peeled off after interaction with CB[7]. All the following experiments were therefore performed after equilibration. The absorption spectra of BODIPYs in PBS with 20% MeCN indicated the presence of strong aggregation (Fig. 3A, B and Fig. S2, ESI†) with a broad Q-band and a very low extinction coefficient. Interaction with CB[7] increased the absorption (indicating better solubility) but the aggregated character was mostly retained although an increased level of monomers could be observed by the changed ratio of bands in the Q-band area (*e.g.*, for **5**, Fig. 3B). No or only weak fluorescence emission was observed without any CB[7] (Fig. 3C, red line). Titration of the BODIPY solution with CB[7] led to a several-fold increase in fluorescence emission (Fig. 3C) clearly indicating that the level of monomers increased. Calculated stoichiometry confirmed the expected ratio between CB[7] and Ad moieties being 1 : 1 (Fig. 3C (inset) and Fig. S6, ESI†). However, the association constant values of these complexes were not determined due to complications with their ultra-high stability combined with low solubility. Subsequently, singlet oxygen production was monitored by water-soluble singlet oxygen scavenger anthracene-9,10-dipropionic acid (ADPA). The rate of ADPA decomposition after irradiation of BODIPYs was typically low without CB[7] while increased upon the host–guest interaction (Fig. 3D and Fig. S3, ESI†). The interaction of BODIPYs with CB[7] also manifested in changes in the lipophilicity of the final complexes. The partition coefficient between *n*-octanol and PBS (log *P*) of BODIPYs decreased substantially in several cases upon interaction with CB[7] indicating that the macrocycle improved their water solubility (Table 1).

The interaction of BODIPYs with CB[7] was further investigated using NMR. In NMR experiments, we selected the BODIPY **5** to investigate which part of the guest interacts with CB[7]. A mixture of DMSO-d_6 and D_2O (1 : 1) had to be used as a solvent to ensure the solubility of both host and guest at the millimolar concentration needed for the experiments. Upon the addition of 0.5 equiv. of CB[7] per Ad unit to the solution of **5**, a new set of signals appeared upfield from the original signals of **5** (Fig. 4B). Ad protons ($\Delta\delta$ up to 0.82 ppm) and protons of alkyls attached to the nitrogen atom next to Ad unit ($\Delta\delta$ up to 0.19 ppm) were shifted most significantly. This clearly showed that one-half of Ad units of **5** is included inside the CB[7] cavity, while the second half remains unbound. The presence of free and bound Ad signals at 0.5 equiv. of CB[7] can be observed due to the host–guest exchange, which is slow on the NMR timescale. The addition of another 0.5 equiv. of CB[7] per Ad unit resulted in the disappearance of free guest signals, indicating that both Ad units of **5** are encapsulated by the CB[7] macrocycle (Fig. 4C). Similar mode of binding, that is CB[7] binds around Ad units, is expected also for other BODIPY derivatives but could not be investigated due to solubility reasons.

All these experiments showed that the Ad moiety is encapsulated inside the CB[7] and that such interaction increases the level of the monomeric active form of lipophilic BODIPYs in PBS. This encouraging result prompted us to continue with the biological evaluation of the photodynamic activity *in vitro* on human cervical carcinoma cells (HeLa).

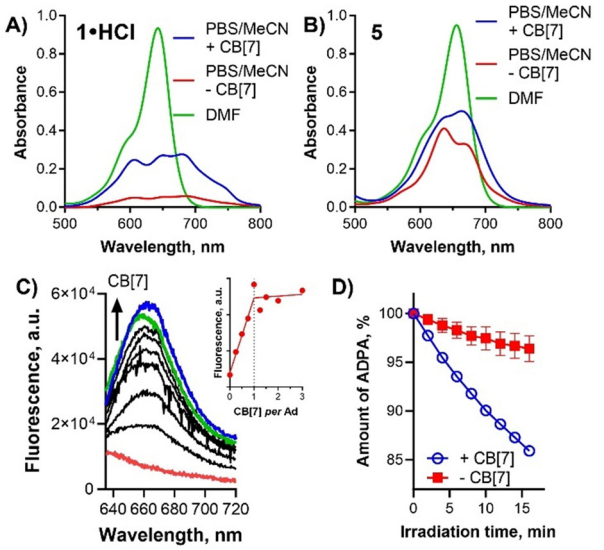

Fig. 3 Absorption spectra (c = 10 μM) of **1·HCl** (A) and **5** (B) in DMF (green) and in PBS containing 20% MeCN with CB[7] (1 equiv. per Ad, blue) or without CB[7] (red). (C) Changes in fluorescence intensity of **1·HCl** (c = 1 μM) in PBS containing 20% MeCN upon addition of CB[7] (red line = 0 equiv., blue line = 1 equiv., green line = 3 equiv. per Ad unit). Inset: Dependence of fluorescence intensity of **1·HCl** on the added CB[7] (monitored at λ_{em} = 661 nm). (D) Decomposition of ADPA by singlet oxygen produced after irradiation of **1·HCl** in PBS containing 20% MeCN with CB[7] (1 equiv. per Ad, blue) or without CB[7] (red). Radiation flux = 62.1 mW.

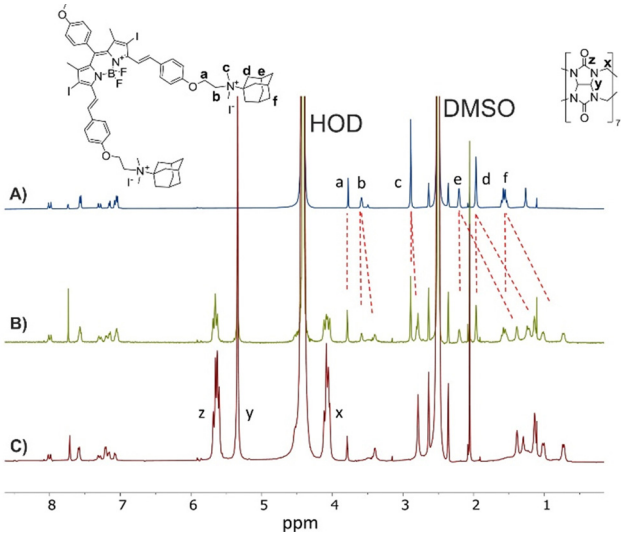

Fig. 4 ^{1}H NMR spectra (500 MHz, DMSO-d_6/D_2O (1 : 1), 30 °C) of **5** (1 mM) in the absence of CB[7] (A) and in the presence of 0.5 equiv. (B) and 1 equiv. (C) of CB[7] per Ad unit.

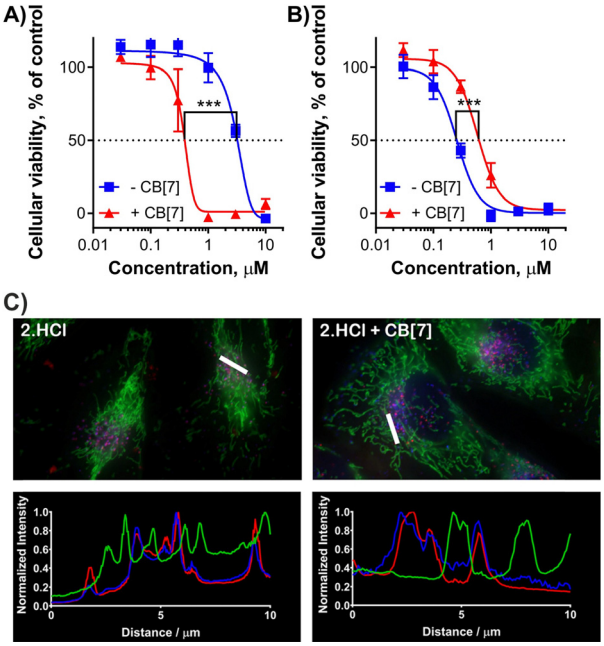

Fig. 5 Photodynamic activity of **2·HCl** (A) and **5** (B) against HeLa cells with (red triangle) or without (blue square) of 1 equiv. of CB[7] per one Ad moiety. Irradiation conditions: $\lambda > 570$ nm, 12.4 mW cm^{-2}, 15 min, 11.2 J cm^{-2}. ***$p < 0.001$. (C) Subcellular localization and intensity profiles of **2·HCl** (red) in HeLa cells without or with CB[7]. The cells were stained for lysosomes (blue) and mitochondria (green). The bar in the images indicates the measured part of an image for the intensity profile and represents 10 μm.

BODIPYs with or without CB[7] were predominantly localized in endolysosomal compartment as was detected with colocalization with a lysosomal probe by fluorescence microscopy (Fig. 5C and Fig. S8–S10, ESI†). Lysosomes may be therefore considered the primary target of singlet oxygen due to their short lifetime. Interestingly, **1·HCl** and **2·HCl** were also partially localized in mitochondria (Fig. S11, ESI†) as low signal colocalized with a mitochondrial probe, but this localization was not affirmed for the complexes of these compounds with CB[7].

Subsequently, the photodynamic activity (expressed as a half-maximum effective concentration, EC_{50}) and dark toxicity without activation (expressed as a half-maximum toxic concentration, TC_{50}) were evaluated. In the dark, no toxic effect was observed for any of the tested samples up to the maximum tested concentration of 30 μM (limit of solubility) regardless of whether incubated with or without CB[7]. Upon light activation without any host, the tested BODIPYs exerted a photodynamic effect with EC_{50} values in the micromolar range. Compound **5** bearing two quaternized nitrogens on styryls was the most active with $EC_{50} = 0.25 \pm 0.03$ μM (Table 2) despite its highly lipophilic character and possible aggregation. Next, BODIPY-CB[7] complexes for testing were prepared to contain one CB[7] per Ad unit (*i.e.*, all Ad units of the BODIPY compounds were engulfed by CB[7]). Upon incubation of the cells with BODIPY-CB[7] complexes, the results significantly differed for BODIPYs containing one and two Ad units. In the case of **1·HCl**, **2·HCl** and **3**, the activity in the presence of CB[7] increased approximately 3–7 times (Fig. 5A, Table 2 and Fig. S7, ESI†) with strong statistical significance supported by the performed unpaired *t*-test. On the other hand, in the case of **4·HCl** and **5**, there was no significant difference (**4·HCl**) between treatment with a single molecule and the complex, or the activity even dropped upon the complex formation (**5**, Fig. 5B).

Following the cytotoxicity results, we focused also on the amount of the compounds present in the cells. The uptake experiments were performed in two independent approaches. In the first one, the cells were incubated with the investigated samples, washed several times, lyzed by Triton X-100 and the fluorescence intensity of the solution was measured (Fig. 6A). Another experiment was based on the fluorescence microscopy of living HeLa cells where uptake was expressed as a reciprocal value of the exposure time of the imaging setup to acquire images with comparable fluorescence intensities coming from the BODIPYs taken up by the cells (Fig. 6B). Similar results were obtained from both independent assays although the absolute values could not be directly compared. The experiments resulted in a general trend where lower uptake was observed

Table 2 Photodynamic activity (EC_{50} values) of studied BODIPYs on HeLa cells[a]

Cpd.	EC_{50} (μM) Without CB[7]	With CB[7][b]	Significance (*p*-value)[c]
1·HCl	6.23 ± 0.71	1.30 ± 0.06	***(0.00027)
2·HCl	3.32 ± 0.36	0.43 ± 0.11	***(<0.00001)
3	1.54 ± 0.40	0.42 ± 0.21	***(0.00012)
4·HCl	1.58 ± 0.64	1.21 ± 0.23	n.s. (0.279)
5	0.25 ± 0.03	0.63 ± 0.11	***(<0.00001)

[a] Data are presented as the EC_{50} values ± the standard deviation. Irradiation conditions: $\lambda > 570$ nm, 12.4 mW cm^{-2}, 15 min, 11.2 J cm^{-2}. At least three independent experiments, each in duplicate, were typically performed. TC_{50} in all cases is over 30 μM (limit of solubility). [b] With 1 equiv. of CB[7] per one Ad unit in the molecule. [c] Statistical significance between samples incubated with/without CB[7] as determined using unpaired *t*-test.

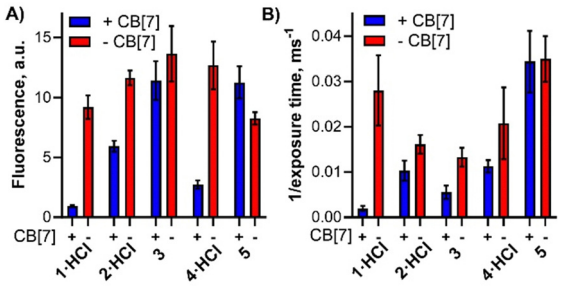

Fig. 6 Cellular uptake of BODIPYs with (blue) or without (red) CB[7] (1 equiv. per Ad) by HeLa cells assessed by two different assays (higher column means always higher uptake). (A) Cells were washed and lyzed by Triton X-100 after incubation and fluorescence intensity was measured. (B) Reciprocal value of the exposure time in fluorescence microscopy of living cells to acquire comparable fluorescence signal.

for the complex with CB[7] than in the absence of CB[7]. It might be a consequence of the larger and too hydrophilic CB[7] lowering the uptake. The results from the uptake study seem to be in contrast with phototoxicity experiments where higher activity was observed for complexes of CB[7] with **1·HCl**, **2·HCl** and **3** despite seemingly lower uptake. However, they must be read together with the results from singlet oxygen production (Fig. 3D) where the complexation improves the production of this cytotoxic species. The final cytotoxicity results therefore might be a combination of two contradictory effects after host–guest interaction (lower uptake but higher singlet oxygen formation) and it depends on which one prevails for a particular compound.

In conclusion, the introduction of the aminoadamantyl moiety into the distyryl-BODIPYs structure generated binding sites for the CB[7] host that formed 1 : 1 complexes with Ad moieties. The encapsulation by CB[7] improved substantially the photophysical properties of lipophilic BODIPYs in water by increasing their solubility and decreasing the formation of aggregates. The interaction was reflected in a higher photodynamic effect for BODIPYs bearing one CB[7] moiety. The supramolecular approach appeared as an efficient way to improve the photodynamic activity of properly designed hydrophobic PSs and may be considered an efficient strategy in the design of novel compounds for PDT. The final effect, however, seems to be a combination of positive (increased singlet oxygen production) and negative (lower uptake by cells) factors. The equilibrium seems to be shifted toward the positive response only for complexes having just one CB[7] moiety.

Author contributions

Jiri Demuth – investigation, Rahul Kaushik – investigation, Magdalena Kozlikova – investigation, Carola Rando – investigation, Miloslav Machacek – investigation, methodology, supervision, Veronika Novakova – supervision, visualization, Vladimír Šindelář – methodology, supervision, funding acquisition, writing, Petr Zimcik – methodology, supervision, conceptualization, funding acquisition, writing.

Conflicts of interest

There are no conflicts to declare.

Acknowledgements

The work was supported by the Czech Science Foundation (20-09212S) and Charles University (SVV 260 664 and PRIMUS/20/SCI/013). V. Š. and C. R. acknowledge the RECETOX Research Infrastructure (LM2023069) financed by the Ministry of Education, Youth and Sports, and the Operational Programme Research, Development and Education. R. K. would like to acknowledge the EFSA-CDN (Reg No. CZ.02.1.01/0.0/0.0/16_019/0000841) and SERB, India for SRG grant (SRG/2023/002022) for financial support. RK also thank the Director, CSIR-NIO for the necessary support.

Notes and references

1 W.-C. Geng, J. L. Sessler and D.-S. Guo, *Chem. Soc. Rev.*, 2020, **49**, 2303–2315.
2 J. Wankar, N. G. Kotla, S. Gera, S. Rasala, A. Pandit and Y. A. Rochev, *Adv. Funct. Mater.*, 2020, **30**, 1909049.
3 L. Xia, J. Wu, B. Huang, Y. Gao, J. Tian and W. Zhang, *Chem. Commun.*, 2020, **56**, 11134–11137.
4 I. Roy, S. Bobbala, R. M. Young, Y. Beldjoudi, M. T. Nguyen, M. M. Cetin, J. A. Cooper, S. Allen, O. Anamimoghadam, E. A. Scott, M. R. Wasielewski and J. F. Stoddart, *J. Am. Chem. Soc.*, 2019, **141**, 12296–12304.
5 X. Zheng, S.-N. Lei, Z. Gao, X. Dong, H. Xiao, W. Liu, C.-H. Tung, L.-Z. Wu, P. Wang and H. Cong, *Chem. Sci.*, 2023, **14**, 3523–3530.
6 C. Sun, H. Zhang, S. Li, X. Zhang, Q. Cheng, Y. Ding, L.-H. Wang and R. Wang, *ACS Appl. Mater. Interfaces*, 2018, **10**, 25090–25098.
7 T. C. Pham, V. N. Nguyen, Y. Choi, S. Lee and J. Yoon, *Chem. Rev.*, 2021, **121**, 13454–13619.
8 Q. Zhang, Y. Cai, X.-J. Wang, J.-L. Xu, Z. Ye, S. Wang, P. H. Seeberger and J. Yin, *ACS Appl. Mater. Interfaces*, 2016, **8**, 33405–33411.
9 L. Kociscakova, C. Rando, M. Kozlikova, M. Machacek, V. Novakova, V. Šindelář and P. Zimcik, *J. Org. Chem.*, 2023, **88**, 988–1002.
10 K. Liu, Y. L. Liu, Y. X. Yao, H. X. Yuan, S. Wang, Z. Q. Wang and X. Zhang, *Angew. Chem., Int. Ed.*, 2013, **52**, 8285–8289.
11 M. González-Béjar, P. Montes-Navajas, H. García and J. C. Scaiano, *Langmuir*, 2009, **25**, 10490–10494.
12 J. Chen, S. Li, Z. Wang, Y. Pan, J. Wei, S. Lu, Q.-W. Zhang, L.-H. Wang and R. Wang, *Chem. Sci.*, 2021, **12**, 7727–7734.
13 H.-B. Cheng, X. Cao, S. Zhang, K. Zhang, Y. Cheng, J. Wang, J. Zhao, L. Zhou, X.-J. Liang and J. Yoon, *Adv. Mater.*, 2023, **35**, 2207546.
14 M. Gupta, K. Parvathi, S. Mula, D. K. Maity and A. K. Ray, *Photochem. Photobiol. Sci.*, 2017, **16**, 499–506.
15 M. A. Alnajjar, J. Bartelmess, R. Hein, P. Ashokkumar, M. Nilam, W. M. Nau, K. Rurack and A. Hennig, *Beilstein J. Org. Chem.*, 2018, **14**, 1961–1971.

16 A. Singh, W.-T. Yip and R. L. Halterman, *Org. Lett.*, 2012, **14**, 4046–4049.
17 O. Buyukcakir, F. T. Yasar, O. A. Bozdemir, B. Icli and E. U. Akkaya, *Org. Lett.*, 2013, **15**, 1012–1015.
18 M. M. Ayhan, E. Özcan, F. Alkan, M. Çetin, İ. Ün, D. Bardelang and B. Çoşut, *Mater. Adv.*, 2022, **3**, 547–553.
19 B. Yuan, H. Wu, H. Wang, B. H. Tang, J. F. Xu and X. Zhang, *Angew. Chem., Int. Ed.*, 2021, **60**, 706–710.
20 J. Zou, Z. Yin, K. Ding, Q. Tang, J. Li, W. Si, J. Shao, Q. Zhang, W. Huang and X. Dong, *ACS Appl. Mater. Interfaces*, 2017, **9**, 32475–32481.
21 M. A. Alnajjar, W. M. Nau and A. Hennig, *Org. Biomol. Chem.*, 2021, **19**, 8521–8529.
22 S. Liu, C. Ruspic, P. Mukhopadhyay, S. Chakrabarti, P. Y. Zavalij and L. Isaacs, *J. Am. Chem. Soc.*, 2005, **127**, 15959–15967.
23 H. He, P.-C. Lo, S.-L. Yeung, W.-P. Fong and D. K. P. Ng, *Chem. Commun.*, 2011, **47**, 4748–4750.